NAVAL
POSTGRADUATE
SCHOOL

MONTEREY, CALIFORNIA

THESIS

TERAHERTZ FREE-ELECTRON LASER OPTICAL DESIGN AND SIMULATION

by

Aaron Zimmer

June 2010

Thesis Advisor: W. B. Colson
Second Reader: R. L. Armstead

Approved for public release; distribution is unlimited

THIS PAGE INTENTIONALLY LEFT BLANK

REPORT DOCUMENTATION PAGE		*Form Approved OMB No. 0704-0188*

Public reporting burden for this collection of information is estimated to average 1 hour per response, including the time for reviewing instruction, searching existing data sources, gathering and maintaining the data needed, and completing and reviewing the collection of information. Send comments regarding this burden estimate or any other aspect of this collection of information, including suggestions for reducing this burden, to Washington headquarters Services, Directorate for Information Operations and Reports, 1215 Jefferson Davis Highway, Suite 1204, Arlington, VA 22202-4302, and to the Office of Management and Budget, Paperwork Reduction Project (0704-0188) Washington DC 20503.

1. AGENCY USE ONLY *(Leave blank)*	2. REPORT DATE June 2010	3. REPORT TYPE AND DATES COVERED Master's Thesis
4. TITLE AND SUBTITLE Terahertz Free-Electron Laser Optical Design and Simulation		5. FUNDING NUMBERS
6. AUTHOR(S) Aaron A. Zimmer		
7. PERFORMING ORGANIZATION NAME(S) AND ADDRESS(ES) Naval Postgraduate School Monterey, CA 93943-5000		8. PERFORMING ORGANIZATION REPORT NUMBER
9. SPONSORING /MONITORING AGENCY NAME(S) AND ADDRESS(ES) N/A		10. SPONSORING/MONITORING AGENCY REPORT NUMBER
11. SUPPLEMENTARY NOTES The views expressed in this thesis are those of the author and do not reflect the official policy or position of the Department of Defense or the U.S. Government. IRB Protocol number _____.		
12a. DISTRIBUTION / AVAILABILITY STATEMENT Approved for public release; distribution is unlimited		12b. DISTRIBUTION CODE A

13. ABSTRACT (maximum 200 words)

The Free Electron Laser (FEL) provides a versatile method for producing laser light. Traditionally, FELs are complicated in design and occupy large research facilities. The primary goal of this thesis is to investigate a particular FEL design that is small in size and operates in the terahertz (THz) frequency regime. The optics materials requirements are explored for power levels ranging from mW to kW. Additionally, as part of a simpler design and in spite of the large amount of diffraction present at THz wavelengths, a waveguide will not be utilized as others have done previously. Laser beam clipping, which is defined as the absorption of the laser beam at the outer edges of the diffracted mode, and a shortened undulator are investigated as methods to support the elimination of the waveguide.

14. SUBJECT TERMS Free Electron Laser, FEL, Terahertz, THz, FEL Simulations, Beam Clipping		15. NUMBER OF PAGES 77
		16. PRICE CODE

17. SECURITY CLASSIFICATION OF REPORT Unclassified	18. SECURITY CLASSIFICATION OF THIS PAGE Unclassified	19. SECURITY CLASSIFICATION OF ABSTRACT Unclassified	20. LIMITATION OF ABSTRACT UU

THIS PAGE INTENTIONALLY LEFT BLANK

TERAHERTZ FREE-ELECTRON LASER OPTICAL DESIGN AND SIMULATION

Aaron A. Zimmer
Lieutenant, United States Navy
B.S., Old Dominion University, 2006

Submitted in partial fulfillment of the
requirements for the degree of

MASTER OF SCIENCE IN APPLIED PHYSICS

from the

**NAVAL POSTGRADUATE SCHOOL
June 2010**

Author: Aaron A. Zimmer

Approved by: William B. Colson
                Thesis Advisor

                Robert L. Armstead
                Second Reader

                Andrès Larraza
                Chairman, Department of Physics

THIS PAGE INTENTIONALLY LEFT BLANK

ABSTRACT

The Free Electron Laser (FEL) provides a versatile method for producing laser light. Traditionally, FELs are complicated in design and occupy large research facilities. The primary goal of this thesis is to investigate a particular FEL design that is small in size and operates in the terahertz (THz) frequency regime. The optics materials requirements are explored for power levels ranging from milliwatts to kilowatts. Additionally, as part of a simpler design and in spite of the large amount of diffraction present at THz wavelengths, a waveguide will not be utilized as others have done previously. Laser beam clipping, which is defined as the absorption of the laser beam at the outer edges of the diffracted mode, and a shortened undulator, are investigated as methods to support the elimination of the waveguide.

THIS PAGE INTENTIONALLY LEFT BLANK

TABLE OF CONTENTS

LIST OF FIGURES

THIS PAGE INTENTIONALLY LEFT BLANK

LIST OF TABLES

THIS PAGE INTENTIONALLY LEFT BLANK

LIST OF ACRONYMS AND ABBREVIATIONS

ARPA	Advanced Research Projects Agency
dB	Decibel
ERL	Energy Recovery Linear Accelerator
FEL	Free Electron Laser
HF	Hydrogen Fluoride
HRFZ	High Resistivity Float Zone
ICBM	Inter-Continental Ballistic Missile
K	Kelvin
KE	Kinetic Energy
Km	Kilometer
LASER	Light Amplification by Stimulated Emission of Radiation
MeV	Mega Electron Volt
MIRACL	Mid-Infrared Advanced Chemical Laser
RF	Radio Frequency
THz	Terahertz
ZnSe	Zinc Selenide

THIS PAGE INTENTIONALLY LEFT BLANK

ACKNOWLEDGMENTS

I would like to thank Prof. Colson for giving time and helpful advice. Your support, understanding, and ability to clearly explain the most complex topic have been paramount to my understanding of directed energy.

To Professor Armstead, thank you for taking the time proofreading and straightening out my scattered thoughts that I optimistically called "rough drafts." Your efforts helped me construct a well-worded, better flowing finished product.

To Professor Blau, thank you for all the help with simulations. Your taking the time to answer my questions and teach me was not required, but was much appreciated.

Additionally, I must thank my three wonderful sisters for their support and encouragement, which has meant so much throughout my Naval career.

Finally, to my wife, Jessica: without you, I would not be where I am today. Thank you for being you.

THIS PAGE INTENTIONALLY LEFT BLANK

I. INTRODUCTION

The Free Electron Laser (FEL) is one of many types of lasers currently in use around the world. It operates on the principle that stimulated emission occurs when an electron is accelerated in the presence of light. Unlike other types of lasers, the FEL is tunable over a wide range of optical wavelengths, which provides an enormous number of possible future uses. In this paper, the use of FELs in the Terahertz (THz) regime is examined, specifically in the range from 100-300 microns and from 10-30 microns, where each range presents its own specific challenges. The absorption, transmission, and reflection of light in these ranges are wholly dependent on the materials used for the optical components in the laser system and on the medium in which the beam is transmitted. Both of these areas are considered further in this thesis.

A. HISTORY

The recent history of lasers dates back to 1960, with the creation of the first LASER by Theodore Maiman at the Hughes Research Laboratory in California.

This small, pulsed laser was a surprise to many in the field who had not considered a pulsed laser beam. However, very shortly after this first pulsed laser's introduction to the world, a second ruby laser, which was well funded by ARPA (the Advanced Research Projects Agency), was made by Ron Martin at TRW [1].

The ruby laser showed its viability up to a power as high as 30 watts; by about 1965, however, it had become

apparent that above that energy level, the ruby laser displayed heat dissipation problems, with the laser rods shattering from the heat.

Around this same time, high-power gas lasers were being considered, with the expectation that troublesome heat could be more easily removed than in a ruby laser. In mid-1965, C. Kumar N. Patel produced a 200-watt 10 μm continuous wave carbon dioxide laser at Bell Laboratories. Later, Hughes reached 1.5 kW with a gas laser which, however, had an extremely low efficiency of ~ 0.1%. Gas lasers continued to make progress and, in 1979, the Air Force put a 400 kW gas-dynamic laser in a Boeing 707—and 2 years later it was able to shoot down an air-to-air missile.

In the 1970s and 80s, the U.S. Navy became interested in chemical lasers, which have a wavelength of ~3-4 μm. In 1978, the 400 kW Navy ARPA chemical laser became the first chemical laser to shoot down a missile in flight. In 1980, TRW completed the first megawatt-class laser, the MIRACL (Mid-Infrared Advanced Chemical Laser). It could emit a 2 MW beam, but only for a few seconds at a time, and thermal blooming was a major issue with beam propagation. Additionally, the laser itself was huge, not portable in any sense.

Enter the Star Wars Era, when lasers received renewed attention for their expected ability to reach into space and knock down ICBMs. In 1991, a 2.7 μm HF laser named *Alpha* finally reached the megawatt class. Then, after

having poured money into laser research with little or no results, United States funding all but disappeared after the fall of the Soviet Union.

The 1990s saw few new laser weapons under development. These were mostly for use in defense against short-range rockets and mortars. Chemical lasers are somewhat effective, but they are too bulky, so current research is re-examining refinements of the original solid-state lasers. Solid-state lasers have now been produced at powers up to 100kW and may be a viable option in the future.

One of the more recent additions to the arena is the FEL. John Madey, of Stanford University, first proposed the FEL in 1970 and subsequently demonstrated one in 1976. Current research has led to a 14 kW FEL at Jefferson Laboratory, and a contract was awarded recently by the Office of Naval Research (ONR) to Raytheon and Boeing to develop the preliminary design of a 100 kW experimental FEL for the U.S. Navy [1].

Currently, there are many FELs in operation around the world, as can be seen in the "Free Electron Lasers in 2008" paper, produced by the Naval Postgraduate School with support from ONR [2]. Experiments probing uses as varied as unobtrusive cargo scanning at shipping ports to wireless power transport into space currently are being considered.

THIS PAGE INTENTIONALLY LEFT BLANK

II. "PARTS LIST" FOR A RECIRCULATING FREE ELECTRON LASER

The Free Electron Laser (FEL) is made up of several components that all work together to create a useable light beam. There are two important players in the FEL: the first is the electron beam and the second is the optical beam. Both are depicted in Figure 1.
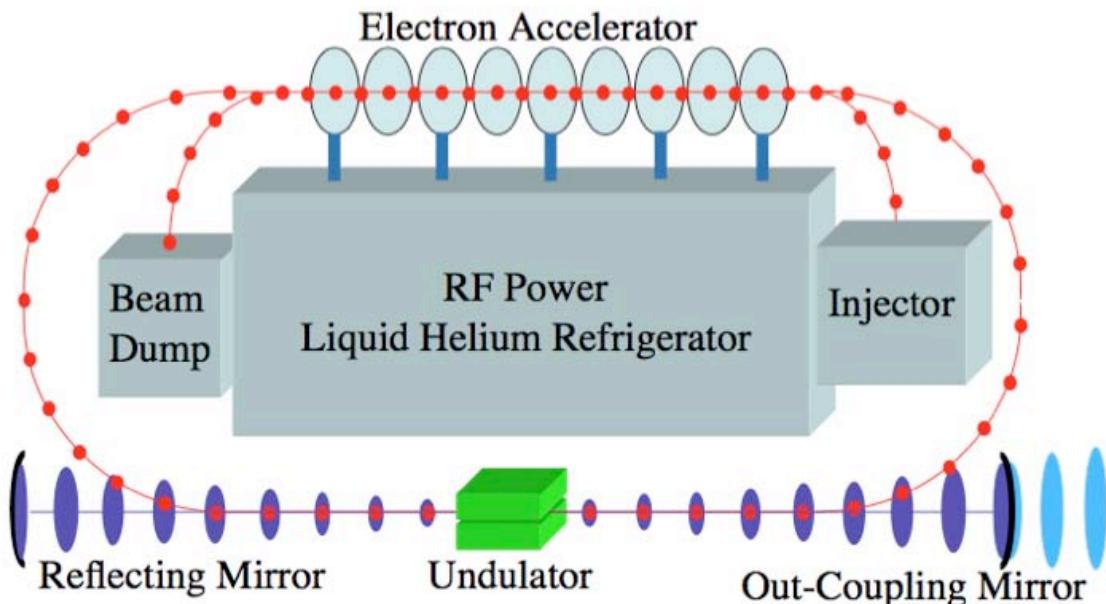
Figure 1. Major parts of a recirculating Free Electron Laser. Electron beam is shown in red, the optical beam is shown in purple and blue. The undulator, shown in green, is where energy is transferred from the electron beam to the optical beam. From [3].

A. ELECTRON BEAM

The electron beam components include the injector, accelerator, beam transport system, undulator, and beam dump.

1.   Electron Injector

Free electrons originate in the injector, provided by thermal emission or photo-emission from the cathode surface. They are then accelerated away from the cathode and into the injector via a static or RF electric field.

2.   Electron Accelerator

Following the initial injection of the electron beam, it goes through a linear electron accelerator.   The electron accelerator uses alternating, intense electric fields, stored in radiofrequency (RF) cavities, to accelerate the charged electrons, increasing their energy. As the electrons leave one cavity, they are synchronized so that they see only continual acceleration.   Electrons come out of different accelerators with energies ranging from a few MeV to thousands of MeV.

3.   Electron Beam Transport

After the accelerator, bending magnets, placed as needed along the red beam line of Figure 1, redirect the electron beam to the undulator. Surrounding the undulator is the oscillator, consisting of a highly reflecting mirror, and an out-coupling mirror. The electron beam is in a nearly perfect vacuum inside a beam pipe.

4.   Undulator

This redirected beam then continues on to the oscillator and travels through the undulator.   The undulator uses a series of alternating magnetic fields, as seen in Figure 2, to wiggle the electrons back and forth

slightly in the transverse direction as they pass through, emitting electromagnetic radiation in the form of light as a consequence.
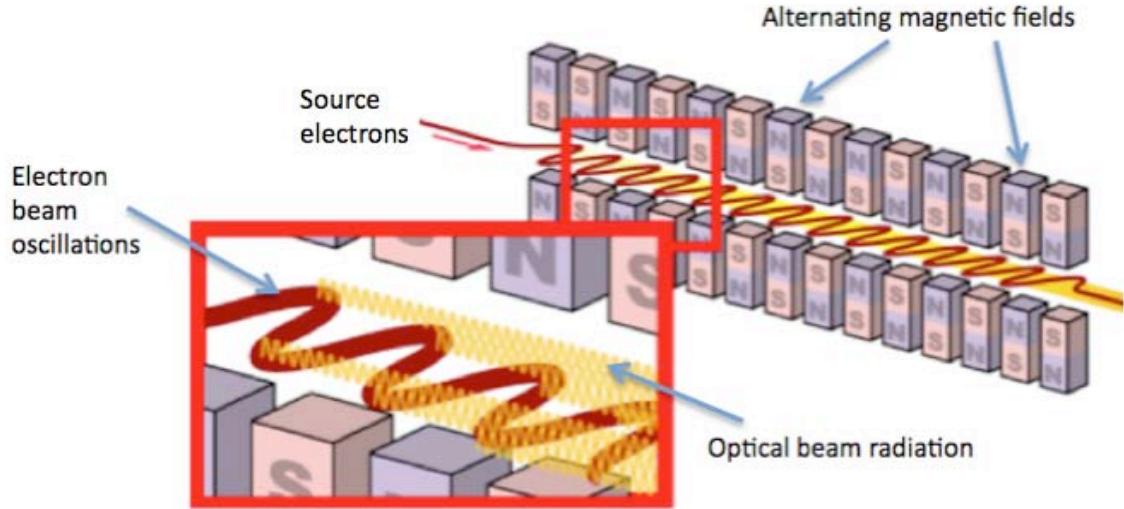
Figure 2.   Major parts of an undulator as used in a FEL. After [4].

This emitted light becomes the basis for the Free Electron Laser "light" beam, as it oscillates back and forth between the reflecting and out-coupling mirrors, which make up the resonator.   The out-coupling mirror is partially transmitting and lets a small portion of the light go through the mirror.   This exiting light is the portion of the light beam that becomes the "pointy edge of the spear" of the FEL.

5.   Beam Recovery and Dump

An additional feature of an Energy Recovery Linear Accelerator (ERL)-type FEL is that there is a low energy beam dump after energy is recovered in the decelerating section.   After the electron beam passes through the oscillator, it continues through bending magnets back to

the electron accelerator, where most of the beam's energy is recovered by sending the electrons through the accelerator cavity 180 degrees out of phase. As the beam slows, this recovered energy is transferred to the intense electric fields within the accelerator and then transferred to the beam now leaving the injector and beginning its positive acceleration.

Any energy left in the waste electron beam is then sent to the beam dump, usually a large piece of copper.

B. OPTICAL BEAM

The optical beam components include the optical beam cavity and optical beam piping to subsequent applications.

1. Optical Cavity

The optical cavity consists of two mirrors placed at the ends of the undulator and maintained in a near perfect vacuum. One mirror is 100% reflecting while the other transmits a small amount of light. The distance between the mirrors is critical and must be constantly maintained to ensure that successive light pulses are kept in phase with the electron pulses while transiting through the undulator. These mirrors must also maintain proper alignment at all times.

2. Optical Beam Piping and Transport

The optical beam is transported and directed via a series of mirrors and lenses.

III. FEL THEORY

A laser is a mechanism for emitting electromagnetic radiation through a process called stimulated emission. A Free Electron Laser can generate coherent, high power radiation, over a large frequency spectrum. This ability to operate over a wide wavelength range is unique among all lasers and allows the FEL to be used for many purposes.

While the FEL consists of many important components, the undulator, illustrated in Figure 3, is its essential distinguishing feature and is where the electron-photon interaction takes place.
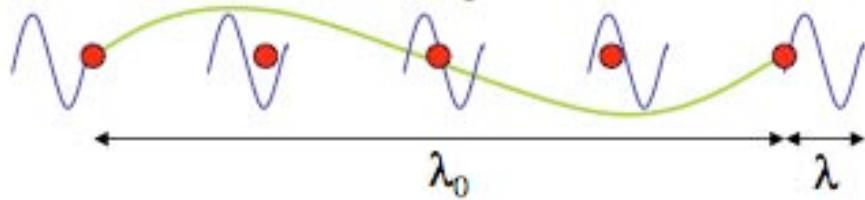
Figure 3.   FEL electron-photon interaction. From [1].

The green line shows one period, λ_0, of the undulator; the blue wave indicates one wavelength, λ, of the optical wave, and the red dot shows the position of the electron relative to the optical wavelength. The electron (red dot) and the optical wave (blue wave) are shown at five intervals as they both pass through the period of the undulator. Inside the optical cavity of the FEL resonator, the electron bunches wiggle through the undulator and emit light. Since electrons cannot travel at the speed of light, the light wave moves forward with respect to the electrons. This is referred to as the *electron-photon race*. Resonance occurs when the light advances by one

9

optical wavelength relative to the electron, for each
oscillation of the electron in the undulator field. This
resonance condition, and the theory of operation for a FEL,
is described below.

A. RESONANCE CONDITION AND PENDULUM EQUATION

The electron motion in an FEL is determined by the
relativistic force equations (cgs units):

$$\frac{d(\gamma\vec{\beta})}{dt} = -\frac{e}{mc}(\vec{E} + \vec{\beta} \times \vec{B}) \,, \qquad\qquad (II.1)$$

$$\frac{d\gamma}{dt} = -\frac{e}{mc}\vec{\beta}\bullet\vec{E} \,, \qquad\qquad (II.2)$$

$$\gamma^{-2} = 1 - \vec{\beta}^2 \,, \qquad\qquad (II.3)$$

where $\vec{v} = \vec{\beta}c$ is the electron velocity, m is the electron
mass, and e is the electron charge magnitude, γ is the
relativistic Lorenz factor, $\vec{E}$ and $\vec{B}$ are the electric and
magnetic fields, respectively.

When an electron enters the undulator of an operating
FEL, the undulator and optical fields together determine
its motion. Substituting the laser and undulator fields
into the Lorenz force equations and realizing that for
relativistic electrons $\beta_z \approx 1$ and that the transverse motion
in the undulator is determined by $\vec{\beta}_\perp = -\frac{K}{\gamma}(\cos k_0 z, \sin k_0 z, 0)$, where
$k_0 = 2\pi / \lambda_0$ and K is the dimensionless undulator parameter, we
arrive at an electron's equation of motion given by

$$\dot{\gamma} = \frac{d\gamma}{dt} = -\frac{e}{mc}E[\beta_x \cos\psi - \beta_y \sin\psi] = \frac{eKE}{\gamma mc}\cos(\zeta + \phi) \,, \qquad (II.4)$$

where $\psi = kz - \omega t + \phi$, E is the optical electric field amplitude in cgs units, ϕ is the optical phase, $k = 2\pi / \lambda$ is the wavenumber, λ is the wavelength, ω is the frequency, and $\zeta = (k + k_0)z - \omega t$ is the electron phase (which is used to measure the electron position on the scale of the optical wavelength (~1µm)).

At this point, it is useful to define the "electron phase velocity" as

$$ v = \dot{\zeta} L / c = L[(k + k_0)\beta_z - k] = \overset{\circ}{\zeta}, \qquad (\text{II.5}) $$

where $(\overset{\circ}{\,})$ indicates a derivative with respect to dimensionless time $\tau = ct / L$ so that τ goes from 0 to 1 along the undulator length, L, i.e., as τ goes from 0 to L/c.

In a beam of electrons, each electron has a different initial phase $\zeta(0) = \zeta_0 = (k + k_0)z_0 \approx kz_0$ as it begins its path through the undulator. The electron's energy changes as seen in Equation (II.4) affect the microscopic position through the electron phase ζ and phase velocity v. Now consider $\dot{v} = L[(k + k_0)\dot{\beta}_z]$ where $\beta \approx 1 - (1 + K^2)/2\gamma^2$ in the relativistic limit ($\gamma \gg 1$). Using this $\dot{\beta}_z$ in the relativistic limit and near resonance (the condition where optimum energy transfer occurs between the electron beam and optical field), we find $\dot{v} = 4\pi N \dot{\gamma}/\gamma$, where N is the number of undulator periods.

This leads to the final dimensionless FEL pendulum equation

$$\mathring{v} = \mathring{\mathring{\zeta}} = |a| \cos(\zeta + \phi) \,, \tag{II.6}$$

where $|a| = 4\pi NeKLE / \gamma^2 mc^2$ is the dimensionless optical field amplitude.

The pendulum equation (II.6) helps identify how in a typical FEL the electrons (~10^6 of them), which are randomly spread over each wavelength in the beam, bunch and radiate coherently. About half of the electrons are moving slightly faster and half are moving slightly slower within each section of the electron beam about one laser wavelength long. A net energy transfer occurs if the electrons have a net change in their average velocities, i.e., the beam bunches at the correct phase, $\delta + \phi = \pi$.

B. WAVE EQUATION

The response of the laser field to the electrons is determined by the wave equation. Start with the full wave equation,

$$\left(\vec{\nabla}^2 - \frac{1}{c^2} \frac{\partial^2}{\partial t^2} \right) \vec{A}(\vec{x},t) = \frac{4\pi}{c} \vec{J}_\perp(\vec{x},t) \,, \tag{II.7}$$

where $\vec{A}(\vec{x},t)$ is the optical vector potential, $\vec{J}_\perp$ is the current source, and c is the speed of light. The laser's electric and magnetic fields can be derived from the vector potential using

$$\vec{E} = -\frac{1}{c} \frac{\partial \vec{A}}{\partial t} \,, \tag{II.8}$$

$$\vec{B} = \nabla \times \vec{A} \,, \tag{II.9}$$

12

Since the laser beam is coherent, $\vec{A}(\vec{x},t)$ has a slowly varying envelope $E(\vec{x},t)$ in the direction of propagation along z, and the slowly-varying, complex optical vector potential can be written in the form

$$\vec{A}(\vec{x},t) = \frac{E(\vec{x},t)}{k}\hat{\varepsilon}e^{i\alpha} \, ,$$ (II.10)

where $\alpha = kz - \omega t$ represents the "carrier wave," $E = |E|e^{i\phi}$ is the complex laser electric field, and $\hat{\varepsilon}$ is the laser field's polarization vector.

Now the wave's amplitude and phase are taken to be slowly varying along the z axis and also slowly varying in time, the left side of the laser wave equation can be written as

$$\frac{\hat{\varepsilon}e^{i\alpha}}{k}\left[\vec{\nabla}_\perp^2 + 2ik\left(\frac{\partial}{\partial z} + \frac{1}{c}\frac{\partial}{\partial t}\right)\right]E = -\frac{4\pi}{c}\vec{J}_\perp \, .$$ (II.11)

After multiplying both sides of the equation by $ke^{-i\alpha}\hat{\varepsilon}^*$ and introducing a coordinate $u = z - ct$ to use the "method of characteristics," the wave equation can be written as

$$\left[\vec{\nabla}_\perp^2 + 2ik\left(\frac{1}{c}\frac{\partial}{\partial t}\right)\right]E = -\frac{4\pi k}{c}\vec{J}_\perp \cdot \hat{\varepsilon}^* e^{-i\alpha} \, .$$ (II.12)

Making substitutions for $\vec{\beta}_\perp$ in $\vec{J}_\perp$ gives

$$\left[\vec{\nabla}_\perp^2 + \frac{2ik}{c}\frac{\partial}{\partial t}\right]E = -4\pi i e K k \rho(\vec{x},t) < e^{-i\zeta}/\gamma >_{(\vec{x},t)} \, ,$$ (II.13)

where $\rho(\vec{x},t)$ is the local electron density in a small volume dV located at position $(\vec{x},t)$ and $\zeta = (k + k_0)z - \omega t$ is again the electron phase, and <> indicates the average value.

13

Now introduce dimensionless time $\tau = ct/L$ where L is the length of the undulator so that $\tau = 0 \rightarrow 1$ during the interaction along the undulator and multiply the wave equation by the factor $-4\pi NeKL^2/\gamma_0^2 mc^2 k$ so

$$\left[-\frac{iL}{2k}\vec{\nabla}_\perp^2 + \frac{\partial}{\partial\tau} \right] a(\vec{x},\tau) = - < je^{-i\zeta} >_{(\vec{x},t)} , \qquad (\text{II}.14)$$

where the dimensionless laser field amplitude is again $|a| = 4\pi NeKL|E|/\gamma_0^2 mc^2$, the complex laser field is $|a| = e^{i\phi}$, the dimensionless FEL current density is $j = 8\pi^2 Ne^2 K^2 L^2 \rho/\gamma_0^3 mc^2$, and assuming that $\gamma \approx \gamma_0$ for all the electrons in the beam and during the entire interaction.

In order to write the wave equation more compactly, we define the dimensionless transverse coordinates $\tilde{x} = x(k/2L)^{1/2}$ and $\tilde{y} = y(k/2L)^{1/2}$, and now $\vec{\nabla}_\perp^2 = \partial_{\tilde{x}}^2 + \partial_{\tilde{y}}^2$, the fully dimensionless wave equation becomes

$$\left[-\frac{i}{4}\vec{\nabla}_\perp^2 + \frac{\partial}{\partial\tau} \right] a(\vec{x},\tau) = -\left\langle je^{-i\zeta} \right\rangle_{(\vec{x},\tau)} , \qquad (\text{II}.15)$$

When diffraction is small and the beams overlap exactly, the FEL wave equation can be written in its simplest form

$$\overset{\circ}{a} = -j < e^{-i\zeta} > , \qquad (\text{II}.16)$$

The dimensionless current density j measures the coupling (and gain) between the laser light and electron beam, $< e^{-i\zeta} >$ measures the average amount of bunching in the beam, and $\vec{\nabla}_\perp^2$ term in Equation (II.15) describes the possible diffraction of the beam. When the bunched electrons start to

remove energy from the optical beam, saturation has been achieved and the growth of the optical field ceases.

THIS PAGE INTENTIONALLY LEFT BLANK

IV. OPTICAL THEORY / ATMSOPHERIC PROPAGATION

Now that the description of FEL Theory is complete, it is important to discuss how the laser light will interact in the atmosphere as it is transmitted. There are four major atmospheric effects as a laser beam is propagated through the atmosphere. These effects can lead to attenuation, broadening, defocusing, and deflection of the beam from its initial propagation path [2]. The four areas of most concern to THz FEL propagation in the atmosphere are diffraction and absorption and, in higher power applications, thermal blooming and turbulence.

A.   DIFFRACTION

In the simplest terms, FEL beam diffraction can be described as the spreading of a Gaussian beam as it propagates. This spreading is caused by the physical property of electromagnetic waves to eventually spread as they propagate and can be easily affected by changing the size of the optical mode waist radius (w_0).

The equation governing the diffraction of an optical Gaussian beam is

$$w(z) = w_0 \left(1 + \frac{z^2}{z_R^2} \right)^{\frac{1}{2}} \qquad (IV.1)$$

where $w(z)$ is the coherent optical mode radius at distance z, w_0 is the optical mode waist, and z_R is the Rayleigh length. The Rayleigh length is determined from

$$z_R = \frac{\pi w_0^2}{\lambda} \qquad (IV.2)$$

where λ is the optical wavelength of the beam. Figure 4 provides a physical representation of how a Gaussian beam spreads with distance.
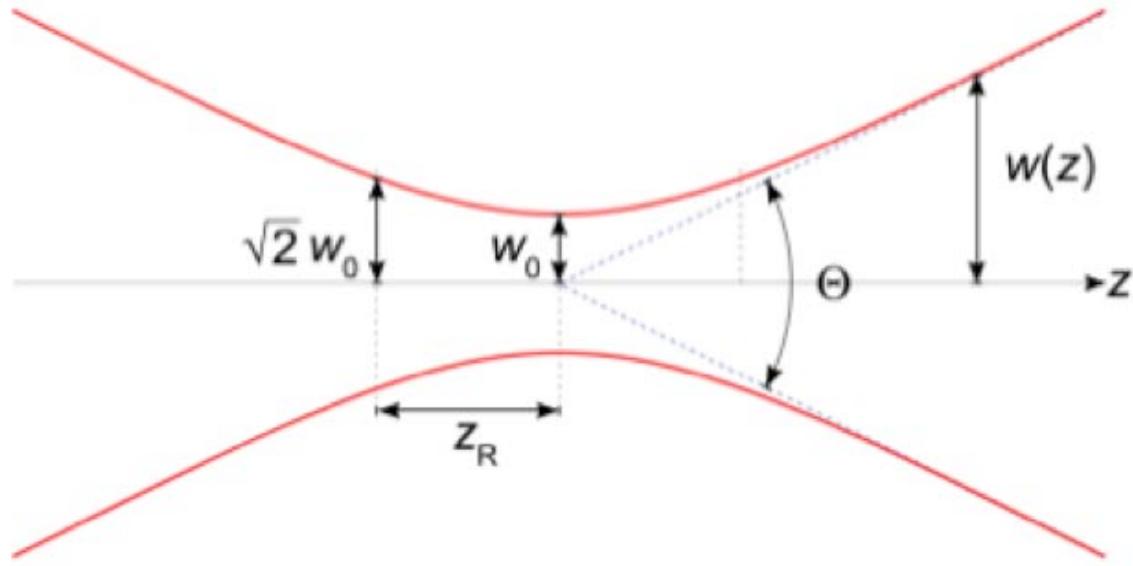
Figure 4.   Optical diffraction of a FEL.   After [5].

   If the approximation is made that the propagation distance z is much greater than the Rayleigh length z_R, then

$$ww_0 \simeq \frac{z\lambda}{\pi} \qquad\qquad (IV.3)$$

and from Equation (IV.3) it is easy to determine that if you hold z and λ constant, then w and w_0 can be adjusted as needed to satisfy the equation.   This ability to manipulate w and w_0 in order to satisfy the diffraction Equation (IV.1) is important for applications where w at distance z is specified so that w_0 determines the aperture size.

18

B.   ABSORPTION

Beer's law best describes absorption of laser beam in the atmosphere

$$\tau = \frac{I(z)}{I_0} = e^{-\alpha z} \qquad\qquad (\text{IV.4})$$

where τ is the transmittance for a distance z, I is the irradiance at z, I_0 is the initial irradiance, and α is the absorption coefficient [2].   It is apparent from Equation (IV.4) that absorption is a process in which energy is removed via interaction with particles that are present in the atmosphere or other medium in which a beam is propagating.   The absorption coefficient is dependent on the frequency of the light being transmitted and the size, number density, and type of the particles present in the transmission path.

A common way to describe atmospheric transmission in the atmosphere is as a loss in decibels (dB) per unit distance.   When doing so, "the absorption of light during wave propagation is often called attenuation" [6].

Figure 5 describes the transparency of the atmosphere at sea level for various wavelengths.   It is apparent that in the range from 300 to 30 μm there is a significant amount of attenuation therefore making FEL operation in the regime impossible at long distances.   As you approach 10 μm, attenuation is much less significant and long-range laser propagation is possible.   Note that weather effects can have a large effect on the propagation distance of a laser beam in the atmosphere.
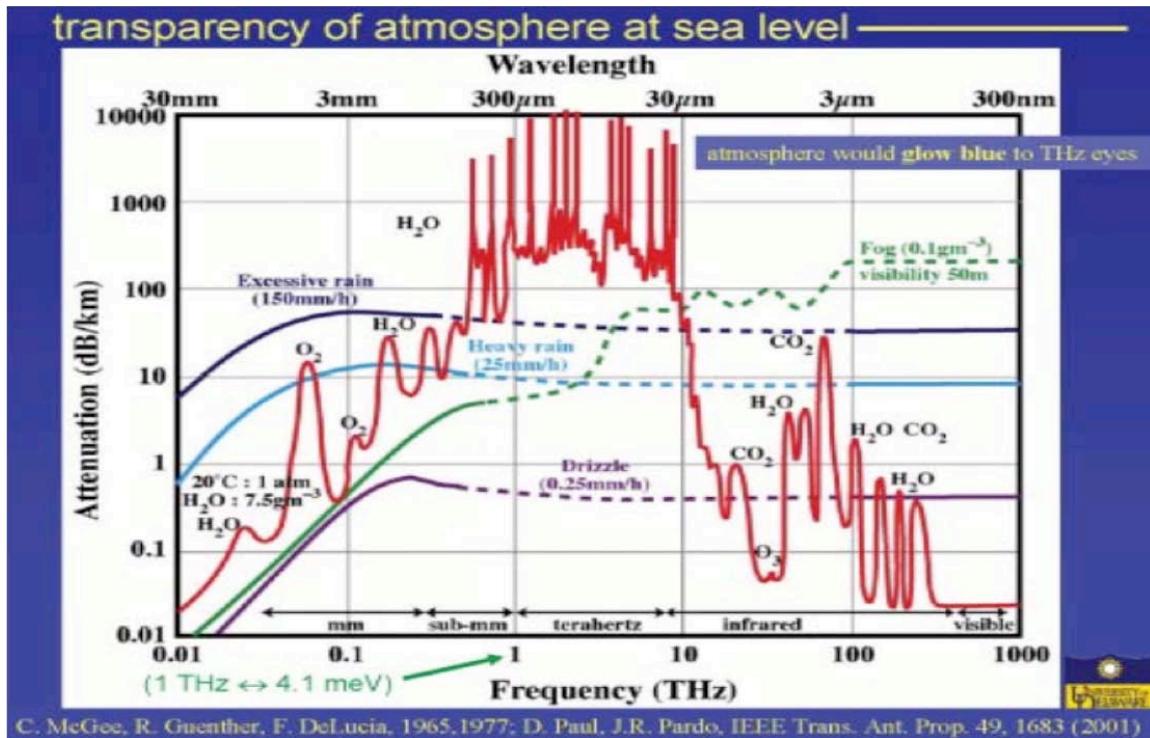
Figure 5.   Transparency of atmosphere at sea level.
From [7].

When considering what distances can be propagated at
in the THz regime, four different wavelengths were explored
for this thesis.   Pulling the approximate values for 50%
atmospheric attenuation (3 dB/km loss) from the red curve
on Figure 5 and applying Equation IV.3 for those four
wavelengths provides the results displayed in Table 1.

Wavelength (µm)	z (3 dB Range)	ww_0 (m²)	If w_0 = 10 cm, then
300	10 m	0.001	w ~ 10 cm
100	30 m	0.001	w ~ 10 cm
30	100 m	0.001	w ~ 10 cm
10	3 km	0.01	w ~ 100 cm

Table 1.   Various ww_0 for different wavelengths

As can be seen from Table 1, as the wavelength is increased from 10 μm to 300 μm, the range achieved before a 3 dB loss occurs increases. In addition, the spot size and/or the optical mode waist (w and w_0) can be adjusted to attain the required value for the application consistent with the value of ww_0. In this scenario, one can either fix the antenna size while varying the size of the beam at the target, or one can maintain a consistent beam size at the target and vary the antenna size. This decision will be made with respect to the application being considered.

C. THERMAL BLOOMING

As the optical power transmitted through the atmosphere reaches the kilowatt level, an atmospheric effect called thermal blooming can become a concern. Thermal blooming is the result of the nonlinear interaction of the FEL's optical beam and the absorption of the beam energy by the atmosphere, thereby heating the air and causing localized density gradients in the medium. These gradients result in the spreading of the laser beam, which spreads the beam and reduces the optical intensity at the target [8]. An illustration of the effect of thermal blooming is provided in Figure 6.
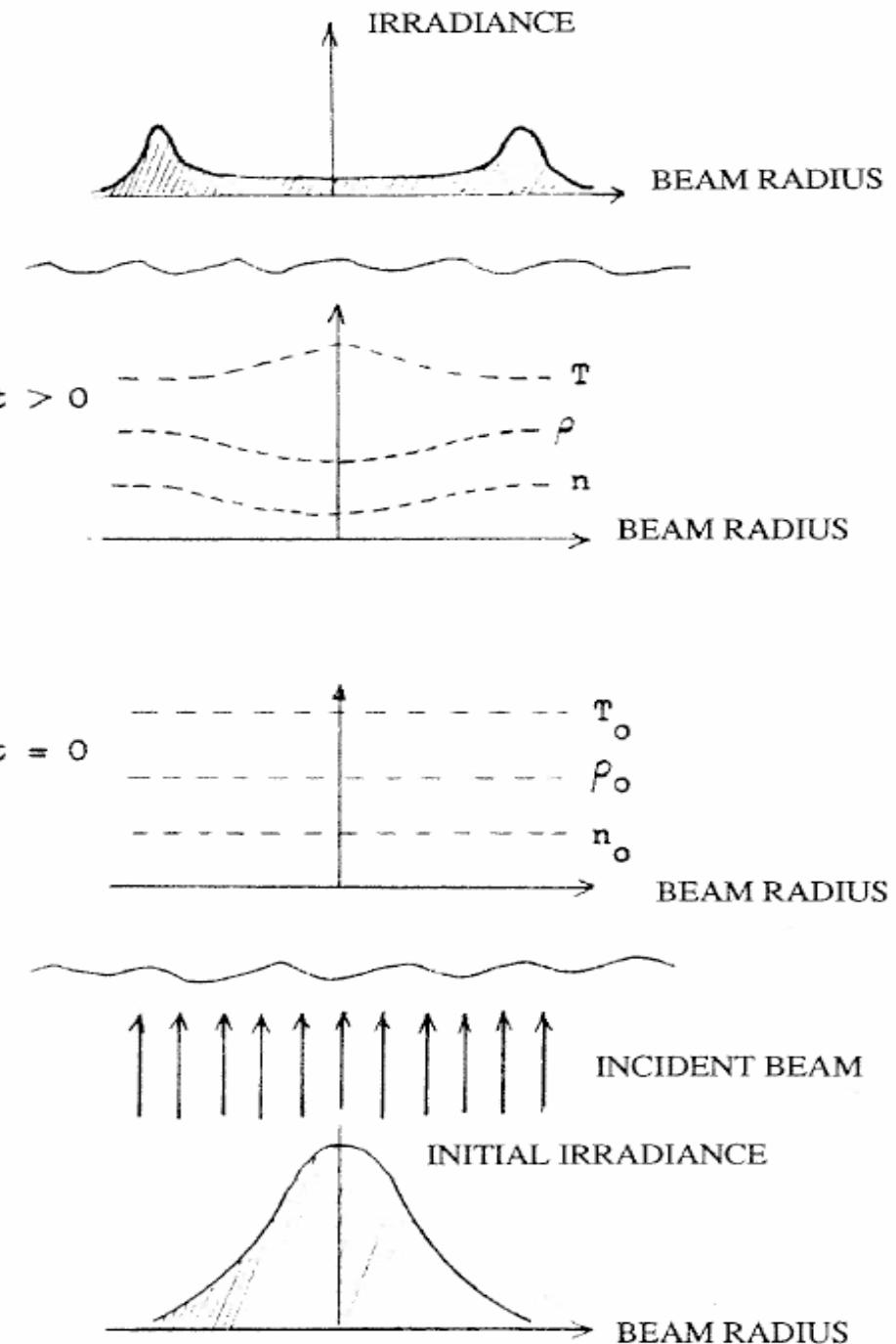
Figure 6. Thermal blooming of a continuous wave beam through stationary atmosphere, where T is temperature of the air, ρ is the mass density of the air, and n is the index of refraction. From [2].

There are a few factors that determine the thermal blooming effect on a laser beam. These include:

1.   Laser beam characteristics, specifically the area

2.   The propagation medium

3.   The dwell time of the laser beam

These factors can to some degree be manipulated to minimize the occurrence of stagnation zones. These zones lead to heating of the stationary air in the center of the beam to higher temperatures than the air at the edges of the beam, which is the cause of the thermal blooming lens [2].

The effects of thermal blooming are of concern only over long distances in an absorptive medium such as the atmosphere. There are several methods that can be used to minimize thermal blooming: The first method is to simply reduce the intensity of the beam, which reduces the heating of the atmosphere and the resulting defocusing. However, this may not work in higher power applications. A second method is to increase the area of the beam, which may work in some cases but not others, such as ship self defense. And a third is to increase the cross movement of the medium in which the beam is propagating, so that the beam slews laterally across the atmosphere, which avoids the blooming effect. With luck there will be a crosswind or the laser platform may move to create its own crosswind, i.e., move perpendicular to the target line of sight.

D.   TURBULENCE

Turbulence is driven by naturally occurring temperature variations in the atmosphere. As an optical beam transmits through the atmosphere, these temperature

variations cause the beam to wander or spread and break up the beam's wave front into smaller, random incoherent beamlets. For many applications, such as ship self-defense, it is important that the optical beam propagate very precisely and predictably at long distances. Adaptive optics can minimize the effects of turbulence while maintaining a highly concentrated, high power optical beam. Adaptive optics is an established method of reducing the effect of turbulence. One method of adaptive optics, currently in use on the U.S. Air Force Airborne Laser (ABL), is a system made of deformable mirrors that compensate for atmospheric turbulence as is occurs [9].

V. OPTICS

A. MATERIAL CONSIDERATIONS

Optical component materials are clearly important in any FEL design, and especially in the THz regime, due to the high levels of absorption of THz radiation that occurs in many common optics materials. As noted before in this thesis, the wavelength range considered to represent the THz regime is broadly defined as 10 to 300 μm, or 1 to 30 THz.

For the transmission and propagation of these wavelengths there are unique challenges that must be overcome with respect to optical components. The preferred optical material will:

1. Transmit a large fraction of the radiation entering the lens or window.

2. Remove the heat absorbed in the lens at a rate equal to its entry into the lens.

3. Expand a minimal amount as it is heated so that lens distortions are kept within reasonable limits.

In order to achieve these goals, several materials are examined and the results are displayed.

The materials considered for THz applications are Single Crystal Sapphire, Crystal Quartz, Silicon, Zinc Selenide, and CVD (Chemical Vapor Deposition) Diamond. Each of these is considered with respect to its thermal conductivity, coefficient of thermal expansion, and transmission of THz frequency radiation.

25

1.   Single Crystal Sapphire

As can be seen from Figure 7, Single Crystal Sapphire has been shown to have good transmission properties at wavelengths from 0.3 μm up to approximately 6 μm [10]. Several other sources of information were explored, but transmission at wavelengths beyond 6 μm was not found. The implication is that the transmission is very poor beyond this wavelength. Due to a lack of data available to determine Sapphires ability to transmit in the area of interest (10 to 300 μm), Sapphire will not be considered further as a possible THz optics material with respect to its thermal conductivity or thermal expansion coefficient [10, 11].
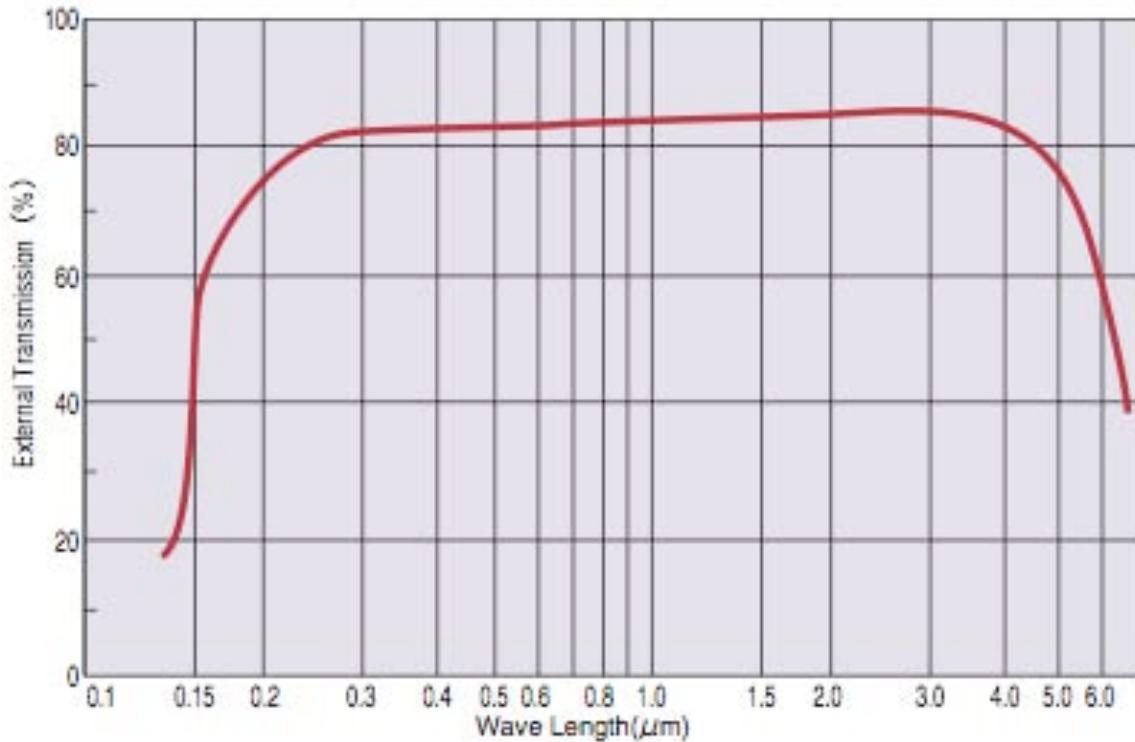
Figure 7.   Optical transmission of a 1 mm thick sample of Single Crystal Sapphire vs. wavelength. From [10].

2. Crystal Quartz

Optical transmission properties of crystal quartz were considered first and are displayed in Figure 8.
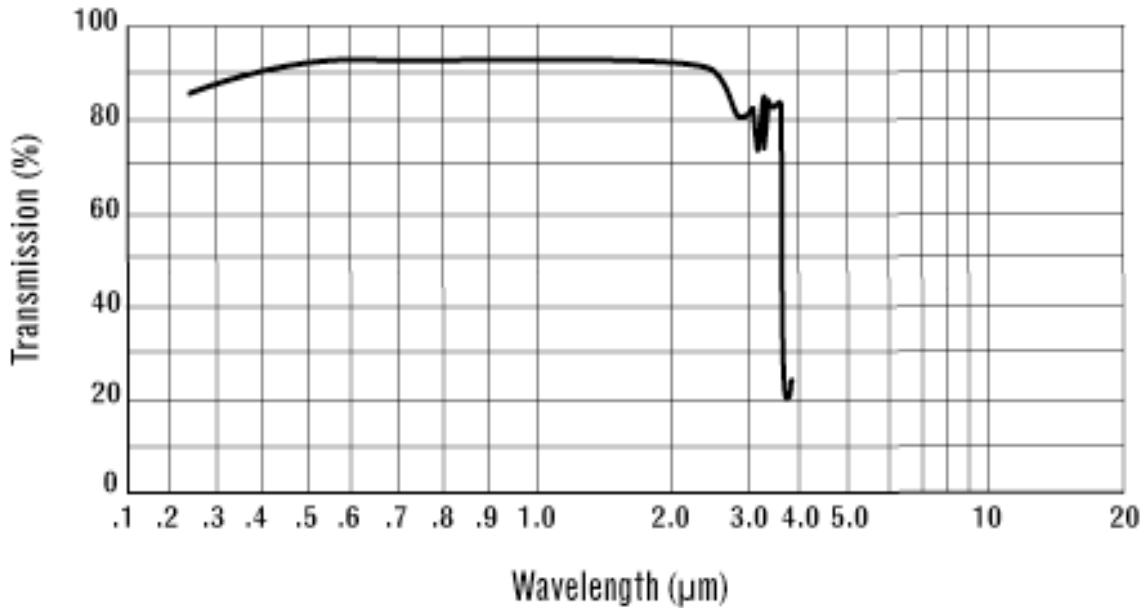
Figure 8.   Optical transmission of a 1 mm thick sample of Crystal Quartz vs. wavelength. From [12].

As with Single Crystal Sapphire, there is a lack of available research to determine Crystal Quartz' ability to transmit in the THz regime.   Therefore, do to the lack of encouraging data, Crystal Quartz will not be considered further as a possible THz optics material with respect to its thermal conductivity or thermal expansion coefficient.

3. Silicon

A specific type of silicon, called "High Resistivity Float Zone (HRFZ) Silicon," has a significant THz

transmission at wavelengths ranging from approximately 50 to 1000 μm; greater than 50% of the radiation passes as can be seen in Figure 9 [13].
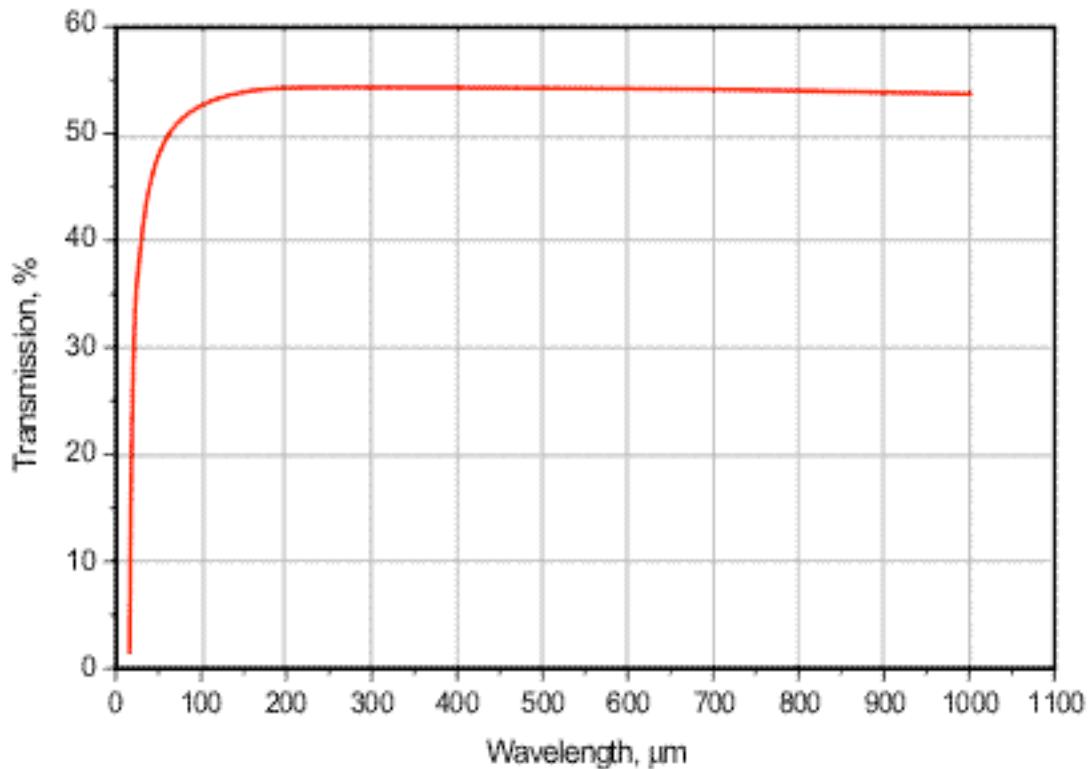
Figure 9.   Optical transmission of a 5 mm thick sample of HRFZ Silicon vs. wavelength. From [13].

However, silicon is a poor thermal conductor (1.5 W/m°C) and is therefore limited to low power operation (only a few watts).   Additionally, silicon's transmission of THz radiation is greatly reduced as temperatures increase above 25 degrees Celsius, as can be seen in Figure 10.   This is an additional factor limiting this material to low power operation.   Data concerning the affect of temperature on the other materials could not be found and is therefore not considered in this thesis.

Transmission Spectrum of Silicon (Si) at Several Temperatures
(5.89mm thickness)
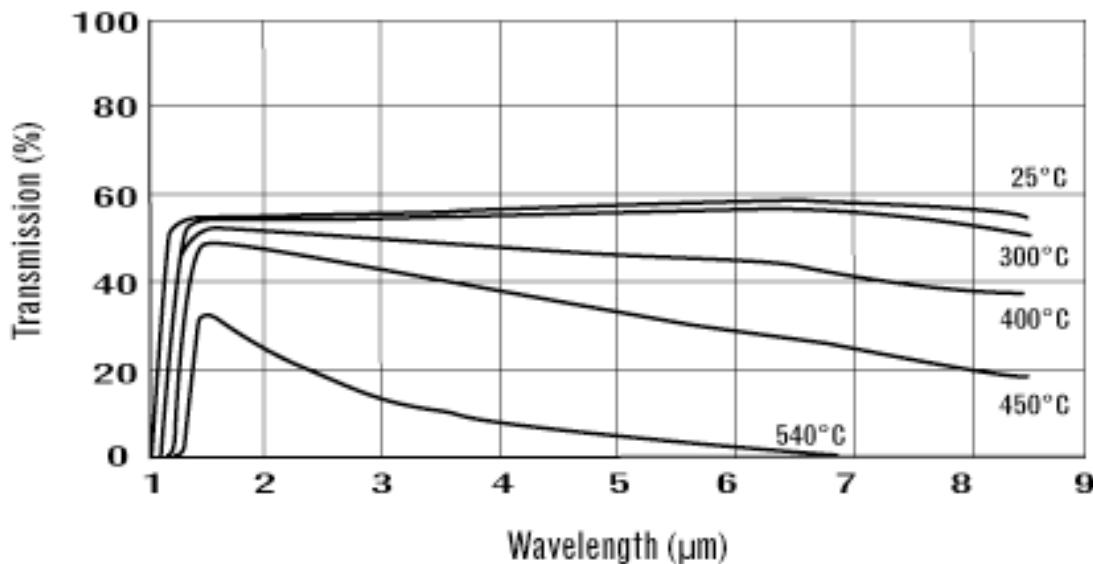
Figure 10.   Optical transmission spectrum of silicon vs.
temperature [11].

4.   Zinc Selenide (ZnSe)

ZnSe turns out to be a very promising material but
only for wavelengths below 20 μm; it does not transmit THz
frequency radiation at wavelengths greater than 20 μm as can
be seen in Figure 11.   The relatively high thermal
expansion coefficient of ZnSe (7.57×10^{-6}) and its poor
thermal conductivity (18 W/m°C) already limits the material
to low power usage (Watts).   Transmission properties of
ZnSe at wavelengths greater than 100 μm were not found. For
low power operations where there is little or no heating,
zinc selenide may be suitable [14].
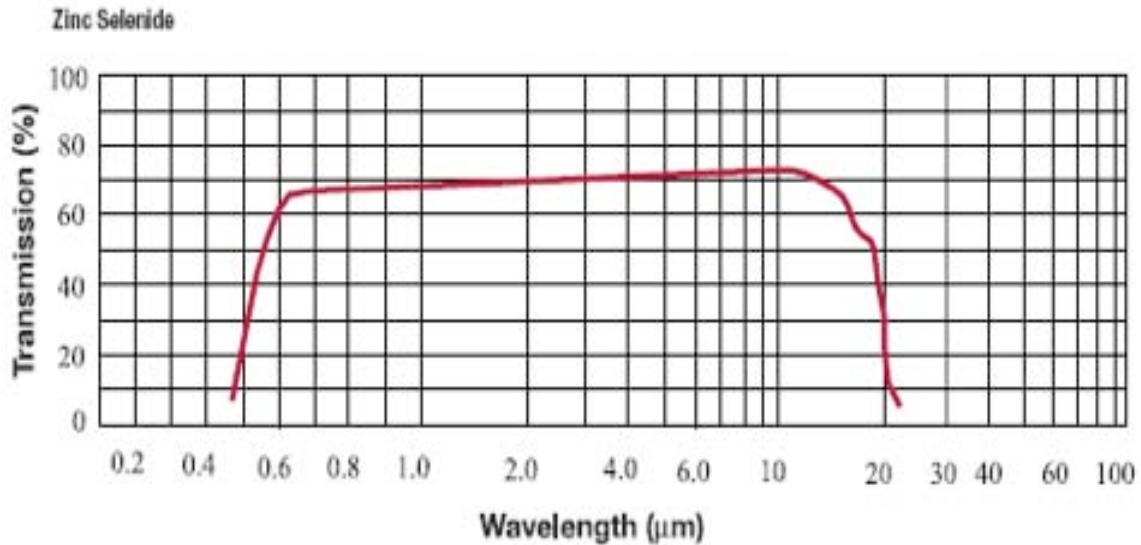
Figure 11.   Optical transmission of a 10 mm sample of
ZnSe vs. wavelength [15].

5.   Chemical Vapor Deposition Diamond

The real winner and obvious choice for THz optics is Chemical Vapor Deposition (CVD) Diamond. CVD Diamond has the highest thermal conductivity of any known natural substance at 3300 W/m°C. It has a very low thermal expansion coefficient on the order of $1\times10^{-6}/°C$, and it has a broad transmission range throughout the THz regime as is evidenced in Figure 12. Additionally, its transmission curve is relatively flat across the entire THz spectrum (10 to 300 μm) at ~ 70% [16, 17].
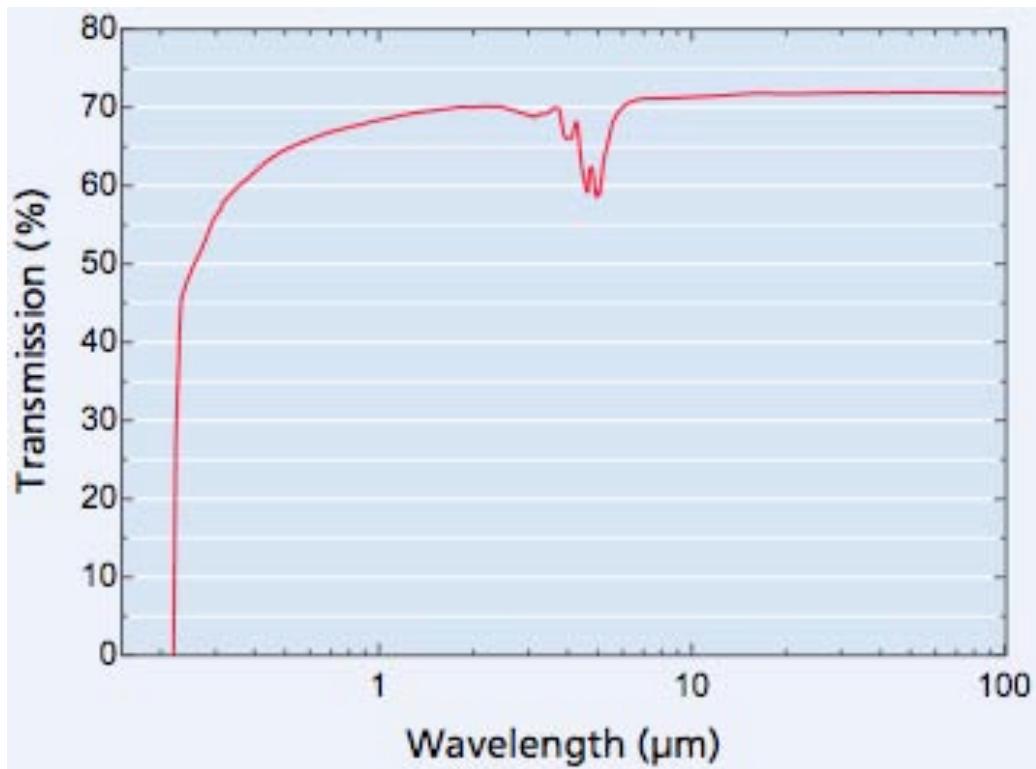
Figure 12.   Optical transmission spectrum of a 1 mm
        thick sample of CVD Diamond vs. wavelength [16].

The only drawbacks to CVD Diamond are its relatively high price, the limited number of manufacturers that currently produce it as an optical grade component, and the lens thicknesses that can currently be produced (on the order of millimeters).   For instance, a 2 mm thick, 5 cm diameter CVD diamond window can easily cost $50,000.

A "stoplight" table, comparing the characteristics of each of the materials, is displayed in Table 2.

Material:	Thermal Conductivity:	Thermal Expansion Coefficient:	Transmission Range:
	(at 20 °C)	$(x10^{-6} / °C)$	(µm)
	(W/m°C)		
HRFZ Si	1.5	2.6	50 – 300
Quartz	1.3	0.59	< 3
Sapphire	42	5	< 6
Zinc Selenide	18	7.57	10 – 20
CVD Diamond	3300	1.2	10 – 300

Table 2.   Comparison of all optical materials considered.

B.   HEAT TRANSFER OUT OF A LENS / WINDOW

At power levels greater than a few Watts, there is a need to maintain the steady-state temperature of the optical components.   The heat removal problem can be simplified and approximated as the radial flow of heat between two coaxial cylinders where a thin slice of these cylinders acts as the lens, as seen in Figure 13.   The curvature of the lens is considered negligible here and no other heat loss mechanism is considered.

32
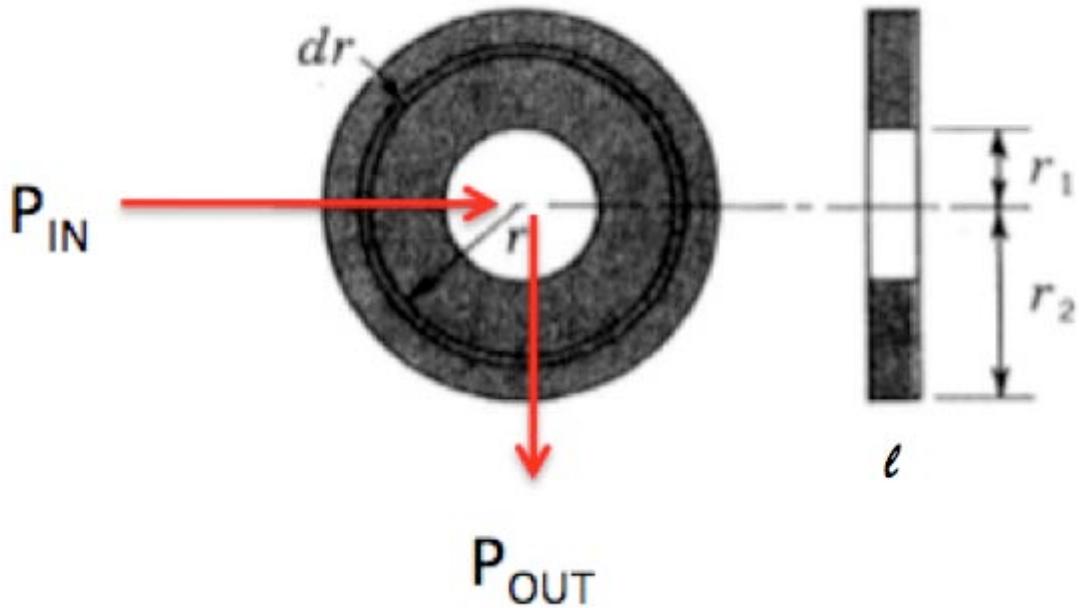
Figure 13.   Heat transfer estimation for a thin lens.
From left to right: front view and side view.
After [18].

The beam is incident on the center of the lens (shown in white) as indicated by r_1 and the full radius of the lens is indicated by r_2.

To determine the rate at which heat is removed from the lens, we start with the equation $\dot{Q} = -k_l 2\pi r l \Delta T / \Delta r$ for heat transfer between two coaxial cylinders [18], where $\dot{Q}$ is the power conducted out of the lens (P_c), k_l is the coefficient of heat transfer, l is the thickness of the lens, and ΔT is the temperature difference across the radius of the lens from r_1 to r_2, and dr is the infinitesimal annular segment of radius.   After integration, the heat removal process for a lens is governed by

$$P_c = \dot{Q} = \frac{\Delta T (2\pi l k_l)}{\ln \dfrac{r_2}{r_1}} \qquad\qquad (\text{V.1})$$

A CVD Diamond lens with the design characteristics below could sustain $P_c = \dot{Q} \approx 600$ watts of continuous heat removal. Taking into consideration that the coefficient of absorption of CVD Diamond is roughly 10% at ~ 10 μm wavelength [17], it is estimated that a ≈ 6 kW optical beam could be designed and operated using CVD Diamond as a lens and window material.

Example: CVD Diamond Window

Spot size radius (r_1)   = 1 cm

Radius of lens (r_2)   = 2.5 cm

Thickness of lens (l)   = 5 mm

ΔT from r_1 to r_2 = 5 °C

k$_{CVD\ Diamond}$ = 33 W/cm°C

From Equation (V.1), it is easy to see that there are several ways to improve the heat removal performance of the lens for a given material. Increasing the thickness of the lens will provide a linear increase in heat removal capability, but will prove troublesome with respect to the linear expansion and the absorption within the lens as it is heated. Another method would be to maintain a larger steady-state temperature difference across the radius of the lens. This would provide an increase in the heat removal capability of the lens, but could potentially also cause problems as the lens distortions become significant across the radius of the lens. A final method of

34

increasing the heat transfer ability of a given lens material is to increase the size of the laser beam spot transmitting through the lens for a given lens radius. This is a possibility that may impact the performance of the laser by a minimal amount depending on the placement of the lens or window along the optical beam. Additionally, this method has a less significant impact on the heat removal performance of the lens because changing the radius of the spot is in Equation (V.1) as a logarithm and is therefore not a linear effect.

C.   LINEAR EXPANSION OF OPTICAL MATERIALS

When considering different optical materials for use as optical lenses and windows in a FEL it is important to account for the axial expansion of a material to prevent interference with the transmission of the optical beam. Prevention of interference occurs by limiting the axial expansion of a material to less than the length of one optical wavelength. Several actions can be taken to limit the thermal expansion and thus the interference of a lens. The first would be to minimize the thickness of the lens, a second option is to limit the temperature difference across the surface of the lens as needed to minimize surface irregularities, and a third option is to choose a material with a low coefficient of expansion.

With respect to limiting the thickness of the lens or window, there is a limit at which the window will no longer be sufficiently strong to maintain the barrier between a high vacuum and atmosphere. Additionally, with respect to

a lens or a window, the thinner a material is, the less power can be removed from it steady state, thus limiting the power rating of the FEL.

The second option of limiting the temperature difference across the lens in order to prevent distortions would succeed in keeping the lens distortion free, but has a negative side effect of limiting the amount of heat that can be removed from the lens, limiting the total power of the FEL.

The third and least restricting option is to choose a material that has a very low coefficient of expansion, which is the approach taken in the material search conducted here.

D.   MAXIMUM ALLOWABLE POWER

When will thermal expansion become a problem? Using CVD diamond again as an example, the wavelength of 10 μm with an allowable linear distortion of ~ 10% of the optical wavelength.   Knowing that the coefficient of linear expansion for CVD Diamond is 1.2 x 10^{-6}/°C and again using a 5 mm thick lens, then the allowed expansion is $(10\%)(10\mu m)/5mm = 2x10^{-4}\%$.   The temperature difference is quickly determined to be $2x10^{-4}\%/1.2x10^{-6}\%/°C$ = 166°C, using $\Delta l/l = \alpha\Delta T$, where α is the coefficient of linear thermal expansion.

Now, Equation V.1 from Section B and taking into account this new ΔT we can determine the maximum amount of heat that can be continuously removed from the same CVD diamond optic. This new value is ~ 11 kW. This means that

a CVD diamond optic with these specifications could transmit an optical beam of ~ 190 kW of power through it with less than 10% axial expansion. From this result one can conclude that it is possible to operate a THz FEL at powers of hundreds of kilowatts with much less than 1 optical wavelength of linear expansion. At 300 μm, allowing for a 10% expansion would mean a calculated ΔT of ~ 5000°C, a temperature that no FEL optic will operate at, therefore linear expansion of the optic will not be the limiting factor in operational design.

E. COMBINED CRITERIA

Now consider combining our criteria into a single formula expressing the maximum power, P_0, sustainable in a lens of thickness l, linear expansion coefficient α, absorption coefficient δ per unit thickness, and thermal conductivity k_l. The lens thickness expression is $\Delta l / l = \alpha \Delta T$ where ΔT is the temperature difference across the lens. Assume that we limit linear expansion to $\Delta l \approx 0.1\lambda$ or less, so the maximum temperature difference can only be $\Delta T \approx 0.1\lambda / l\alpha$ or less. This temperature difference limits the power conducted away to: $P_c = 2\pi l k_l \Delta T / \ln(2)$, assuming $r_2 = 2r_1$. In steady state operation, the power conducted out must equal the power absorbed, $P_{abs} = P_c$, and the power absorbed is estimated by $P_{abs} = P_0(1 - e^{-\delta l})$. So the single formula describing the limiting power incident on the lens before expanding by ~ $\lambda / 10$ is estimated by

$$ P_0 = \frac{\lambda k_l}{\alpha(1 - e^{-\delta l})} \ . \qquad\qquad (\text{V.2})$$

As an example, CVD diamond is limited to $P_0 \approx$ 40 kW at 10 µm wavelength for a lens of l = 3 mm thickness. This is far above our requirements.

VI. DESIGN PROPOSALS

As shown in Chapter IV, propagation through the atmosphere at long wavelengths (>100 μm) is less successful than at short wavelengths. Therefore, any long wavelength design will be limited to propagation distances of tens of meters before half the power is attenuated. As the wavelengths shorten and approach 10 μm, transmission ranges on the order of kilometers are possible, making it practical to consider power levels on the order of kilowatts.

As part of the desire to keep the THz FEL design simple, a number of steps will be taken. Commercial parts will be used when possible. No drive laser or waveguide will be used. The usual temptation is to use a waveguide inside the undulator at wavelengths of 100 μm or greater in order to minimize diffraction. This design also uses energy recovery of the beam without complete recirculation and bending arcs of 2 x 180°. The FEL can be superconducting, but at 4K versus the more complicated and expensive 2K operation. This design also calls for low beam energy and good mode quality to ensure the beam is useable for laboratory purposes [19].

The absence of a waveguide will result in a limit to the length of the undulator. Diffraction in a long undulator, without scraping, would require too large a gap between the magnets. A large gap reduces the magnetic field in the undulator, thus reducing gain. Diffraction of the long wavelength optical beams may cause the optical

beam to scrape the undulator and be absorbed, or clip the optical mode wings. This presents a conflict in determining undulator length: For larger gain, a longer undulator is desirable (because $gain \propto N^3$), but at longer wavelengths diffraction significantly reduces gain. However, at lower electron beam energies, γ also decreases and since $gain \propto 1/\gamma^3$ it is possible to get respectable gain by keeping γ low, while using a shorter undulator. A ~ 100 period undulator is now common, but we consider 10 periods or less. In the case of longer wavelengths (~ 100 µm), this appears to be the only option for successful operation without a waveguide.

A. DESIGN CHARACTERISTICS COMMON TO ALL WAVELENGTHS

The following design criteria are well established and will be held constant for all further designs discussed in this thesis:

$$\bar{I} \sim 0.1 \text{ A}$$

$$\Delta t_b \sim 5 \text{ ps}$$

$$q = 0.2 \text{ nC}$$

$$f \sim 500 \text{ MHz}$$

$$\lambda_0 \sim 3 \text{ cm}$$

$$K \sim 1$$

$$g \sim 1.2 \text{ cm}$$

where $\bar{I}$ is the average electron beam current, Δt_b is the pulse length, q is the charge of each pulse, f is the frequency of electron pulses, λ_0 is the period of the undulator, K is the undulator parameter (which is

proportional to the strength of the magnetic field in the undulator), and g is the gap of the undulator.

1.   ~ 10 Micron Wavelength Range Design

Beginning with the well-known equation for the mass-energy relationship ($E_b = \gamma m c^2$) we get

$$\gamma = \frac{E_b}{mc^2} \qquad \text{(VI.1)}$$

where E_b is the electron beam energy, m is the electron mass, and c is the speed of light. Using Equation (VI.2), which describes the resonance condition for a relativistic electron beam, it is clear that as γ increases the wavelength of the optical beam will decrease, giving

$$\lambda = \frac{\lambda_0 (1 + K^2)}{2\gamma^2} \qquad \text{(VI.2)}$$

Now, if K is a constant of ~ 1, and λ_0 is also a constant of ~ 3 cm, and an optical wavelength λ of ~ 10 µm is desired, then a beam energy of ~ 30 MeV is desired.

In this wavelength regime, optical radiation at ~ 10 µm propagates easily through the atmosphere and optics are easy to find due to the many types of lasers already in operation. Conveniently, a standard undulator (of ~100 periods) can be used with satisfactory optical beam performance, due to the low level of diffraction present. During the course of this research, it became apparent that many of the issues for this wavelength range can be solved relatively easily with off-the-shelf products, and

therefore this thesis will not investigate further into design solutions for this wavelength.

2.   ~ 30 Micron Wavelength Range Design

Using the same analysis as in Section 1, but using a wavelength λ of ~ 30 μm, a calculated beam energy of roughly ~ 20 MeV is required.   Like the ~ 10 μm range previously, this part of the THz frequency spectrum is less challenging from a design standpoint because the diffraction is not large enough to require a non-standard length undulator.   Beam clipping or scraping (the loss of power from the optical beam due to impingement on the undulator ends) is not serious.

3.   ~ 100 Micron Wavelength Range Design

Again, following the above process to determine the beam energy required for operation, using a λ of ~ 100 μm, a calculated beam energy of ~ 10 MeV is desired.   At this wavelength, clipping of the beam begins to become a limiting factor on operation, while using a standard length undulator.   The useful transmission distance through the atmosphere starts to severely limit the applications for such a beam. To minimize the optical power lost, shorter undulator designs and the effects of beam clipping and scraping become more serious and will need to be considered.

4.   ~ 300 Micron Wavelength Range Design

Using the same process as in the previous three cases, the beam energy required for operation, using a λ of ~ 300 μm, is determined to be ~ 5 MeV.   Taking into account

diffraction, this design will require serious consideration
of undulator length and the effects of clipping/scraping.
With a standard-length undulator, the optical beam would be
so severely clipped that it would fail to operate. It has
been shown, however, that respectable gain can still occur
in as few as six undulator periods, while the shortened
undulator design minimizes beam clipping. Chapter VII will
investigate further the effects of clipping on beam power
and in consideration of undulator design.

As with the ~ 100 μm range radiation, the longer
wavelengths of the ~ 300 μm range radiation do not propagate
long distances without losing much of the power density to
diffraction and extinction in the atmosphere. This serves
to limit the applications for a FEL at these frequencies.
Additionally, optics problems that are well understood for
the shorter wavelengths are not easily solved in this
range. This makes this design problem significantly more
demanding.

B.   TABLE OF PARAMETERS

A compilation of the above designs is displayed in
Table 3.

λ (μm)	γ	E (MeV)
~ 10	~ 59	~ 30
~ 30	~ 39	~ 20
~ 100	~ 20	~ 10
~ 300	~ 10	~ 5

Table 3.   Desired energies to attain wavelengths of
interest.

It is clear that for FEL designs at wavelengths of 100 μm or longer, there will have to be a compromise between beam clipping and a shortened undulator. The following chapter investigates further the effect of clipping through the use of computer simulations.

VII. CLIPPING SIMULATION RESULTS

This chapter does not simulate the designs discussed in the previous chapter. In order to do that, a 4D code is needed and is now being developed. This chapter takes advantage of the NPS 3D Oscillator FEL Code that is available now. The current 3D code uses the Lorentz force equations and the parabolic wave equation to simulate the motion of the electrons as they pass through an electromagnetic field. The code follows the electron path in the optical cavity and includes known losses, as well as allowing the required number of undulator passes to reach steady state [20].

Beam clipping/scraping is the complete removal of the optical beam that intersects an absorbing material placed in the beam pipe. This occurs due to the diffraction of the optical beam, which increases with wavelength. For this simulation, the optical beam is removed on contact with the circular absorber placed at the ends of the undulator resulting in an additional loss in the resonator system.

The 3D code was altered to include this effect in order to determine the affects on the performance of the FEL. There are four clips per pass: the first occurs as the optical beam exits the undulator, the second when it re-enters the undulator after reflecting off of the partially transmitting mirror, the third when it exits the opposite end of the undulator, and the fourth when it returns into the undulator after reflecting off of the fully reflecting mirror. Due to the increased diffraction

caused by each clip, each successive clip enhances the clipping at the next location. The radius of the circular absorber is determined by specifying the fractional power dP/P that would be removed from the fundamental mode passing through the end of the undulator. The fraction of the theoretical fundamental mode clipped is symbolized as dP/P. The effect of clipping was studied for both strong and weak optical fields.

Dimensionless parameters were selected in the 3D code leading to a gain of approximately 80%, and a Q value giving 5% loss per pass, a mirror separation distance of ten times the undulator length, and twenty undulator periods, and a Rayleigh length that is one third of the undulator length.

A.   WEAK FIELD GAIN

The NPS 3D FEL Oscillator code is used to determine weak field gain to evaluate the startup mechanism. In weak optical fields, where the dimensionless optical field is $|a_0| < \pi$, the system has not reached saturation and extraction η is small. Weak field gain, which is defined as the fractional increase in optical power/pass, is of interest to determine whether the FEL will start from spontaneous emission; weak field gain/pass must exceed the round trip loss/pass now including the clipping loss. The weak-field gain of a FEL is determined by running the 3D codes over many passes until gain/pass is constant [21].

The 3D code outputs reported here determine the effect of beam clipping, including the initial phase velocity of the electrons v_0, gain G, extraction η, and optical mode

shape. These simulations assume a long pulse and do not model a particular FEL; they are used to study the effects of clipping and cannot simulate all actual effects. Figures 14 and 15 indicate the results of these simulations for weak fields.
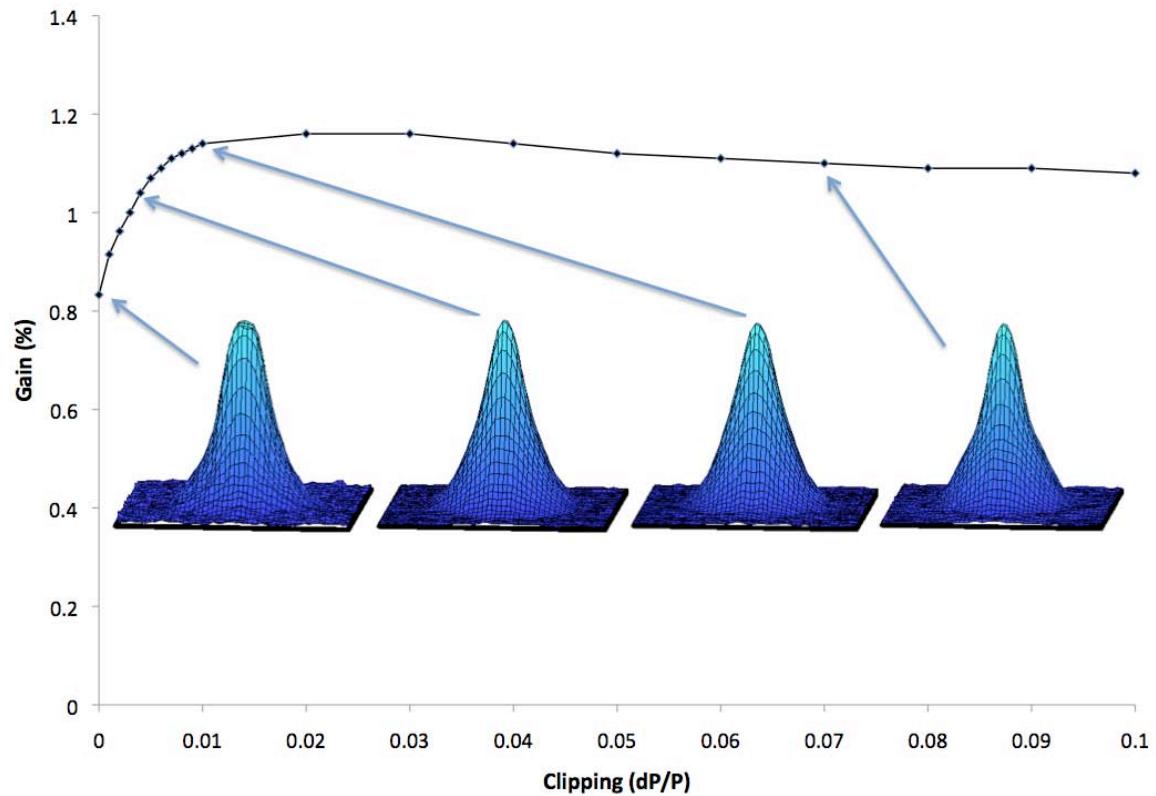

Figure 14.   Weak optical field gain vs. optical beam clipping.

The optical mode shape of the beam was inlaid on the graph of gain G versus clipping percentage dP/P for weak fields at four different clipping percentages in order to illustrate how clipping effects the mode shape. The optical mode to the far left occurs when there is no clipping/scraping and is very close to the theoretical fundamental Gaussian mode defined by the resonator cavity. As the amount of clipping is increased, the optical mode

47

shape becomes more pointed (or focused around the electron
beam) and finally develops a slight "shoulder" as seen in
the far right optical mode. As the clipping parameter dP/P
is increased from 1% to 10%, the optical mode shape
increasingly departs from the original fundamental mode and
is composed of a few higher order modes. At greater than
10% clipping there is sufficient loss so that ~ 80% gain is
not enough to sustain the FEL.
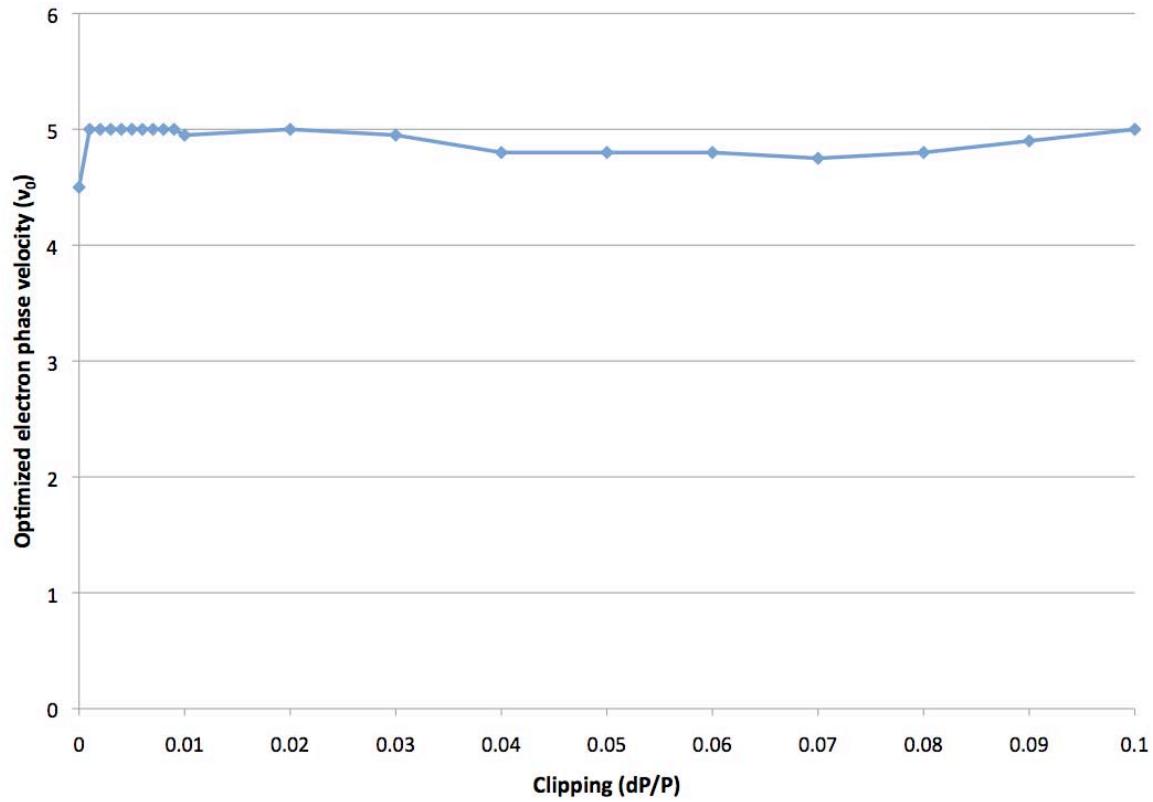
Figure 15.   Optimal electron phase velocity v_0 vs.
                 optical beam clipping for weak fields.

Once the clipping starts, the optimal v_0 shown in
Figure 15 quickly levels off and remains relatively
constant. Clipping appears to have little affect on the
optimal electron phase velocity v_0.

B.   STRONG FIELD EXTRACTION

In strong fields, the FEL reaches saturation quickly over a few hundred passes and the extraction η becomes constant in steady-state. Figures 16 and 17 indicate the results of strong optical fields at steady-state saturation.
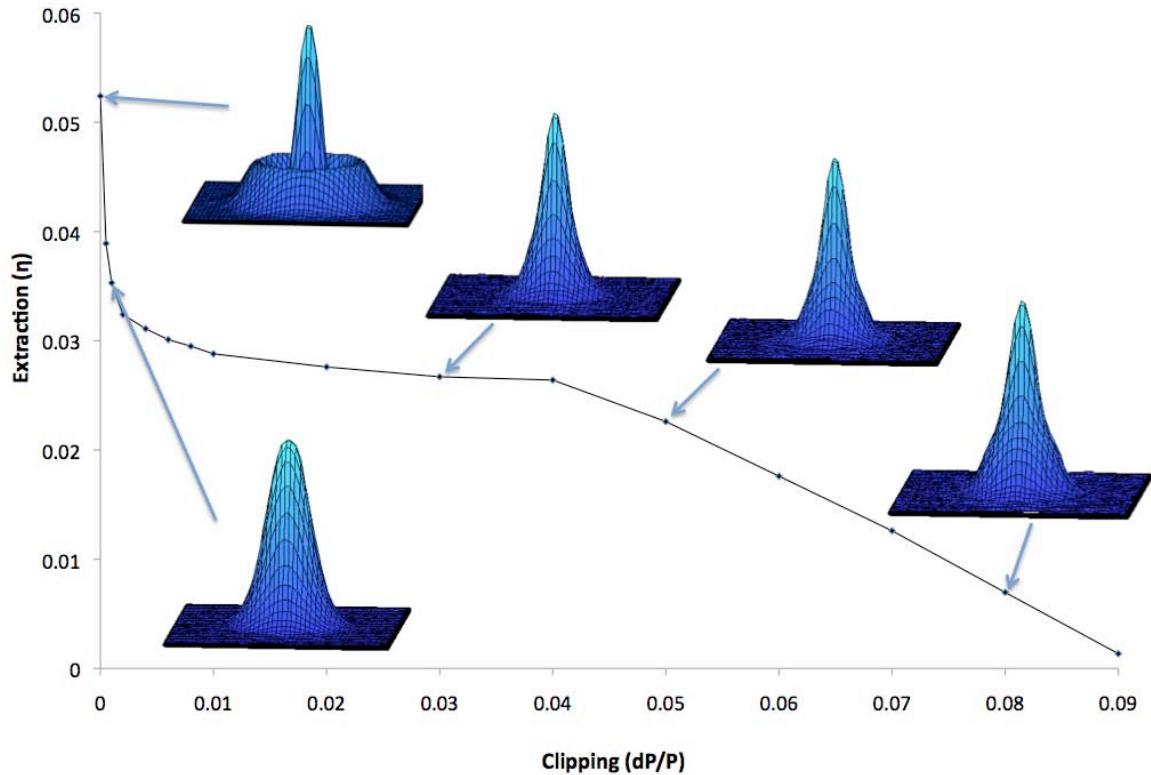

Figure 16.   Strong optical field extraction η vs. optical beam clipping.

The optical mode shape of the beam is inlaid on the graph of extraction versus clipping for strong fields. The five examples illustrate how clipping affects the mode shape. As the optical mode shapes are viewed from left to right some interesting changes occur. A large departure from the fundamental mode is prevalent at dP/P = 0%, but quickly disappears with only a small amount of clipping.

49

This indicates that a very small amount of clipping can quickly eliminate these secondary modes. At dP/P = 0.1%, the resulting optical mode shape most closely matches the Gaussian fundamental mode shape. As dP/P increases from 0.1% to 9%, the optical mode shapes behave similarly to that in weak fields: it becomes more pointed and develops a shoulder. During this progression, the simulation is picking combinations of modes to maximize power, something that occurs naturally in the FEL. One conclusion is that a small amount of clipping does a lot to keep the optical mode shape in the fundamental mode.
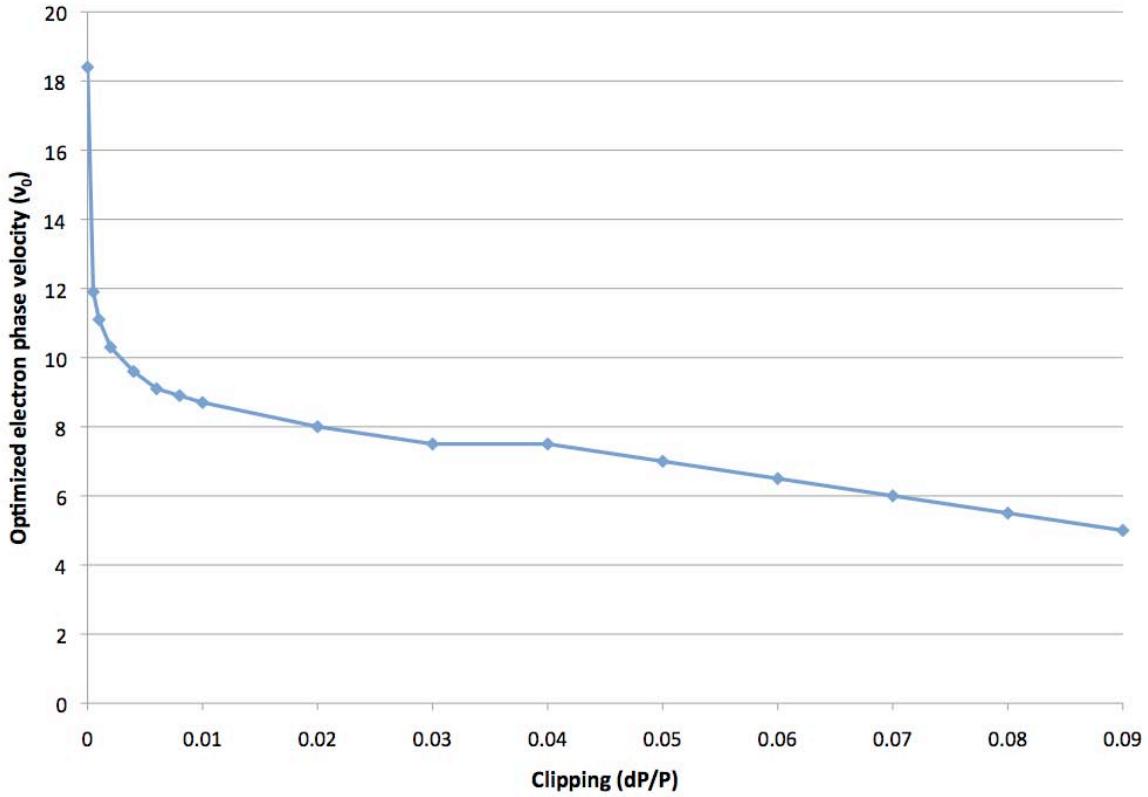

Figure 17.   Optimal electron phase velocity v_0 vs. optical beam clipping for strong fields.

Figure 17 plots the optimum value of the electron phase velocity v_0 versus dP/P.   In the case of strong

fields, an interesting result occurs at dP/P = 0%. The optimal v_0 jumps significantly to large values. This may not be what an experiment would experience because this simulation does not take into account all of the real effects that impact operation, such as the finite optical pulse length and slippage. After the initial jump in the optimal v_0, the value of v_0 quickly levels and remains relatively constant as dP/P increases to 9%.

For each figure, the FEL stops operating at a dP/P of ~ 10%. It is clear that the dP/P parameter cannot be simply viewed as an additional loss in the FEL resonator. First of all, when the clipping absorber is encountered and the outer wings of the mode are removed, diffraction to an even larger mode area will occur when propagating to and from both mirrors and along the undulator. So, one encounter with clipping dP/P ~ 10% results in clipping more than 10% at subsequent encounters. Secondly, the clipping absorber is encountered four times each pass. So, actual steady-state clipping of ~ 20%/encounter may explain the saturation observed.

THIS PAGE INTENTIONALLY LEFT BLANK

VIII.   CONCLUSION

There have been many improvements to Free Electron Laser operation since John Madey proposed the original FEL in 1970. There are many considerations in the design of a new high-energy laser system, and this thesis has begun to address the area of optical component design and the effects of undulator clipping/scraping for an FEL operating in the 1-30 THz regime.

Some materials are found that can successfully operate in the THz regime at power levels ranging from milliwatts to kilowatts. Until now, there has been only limited research in optical properties in the THz regime at the higher powers suggested in this thesis. Absorption coefficients and transmittances are needed for the entire THz spectrum considered here. Many materials were considered, but many other materials were not considered due to lack of available data. To continue this research it is essential that accurate and complete data be available, and this is a suggested area of continued research.

Existing FEL simulation codes will provide many answers to the design requirements for any future FEL. The clipping effects considered in the simulation section of this thesis suggest potentially beneficial changes that could be incorporated into future FELs. It is important to verify these results by the NPS 4D FEL oscillator code now under development. The results of the optical beam clipping/scraping simulation indicate that there may be a positive effect from a small amount of beam clipping on the

beam piping at the exits of the undulator, illustrated by
the reduced number of optical modes present in the optical
beam following a small amount of beam clipping.

LIST OF REFERENCES

[1] W. B. Colson, "Free electron lasers & accelerator physics," PH-4055 Class Notes: Naval Postgraduate School. Monterey, CA, 2009.

[2] H. Weichel, *Laser Beam Propagation in the Atmosphere*. Bellingham, WA: SPIE Optical Engineering Press, 1990.

[3] W. B. Colson, PH 4911 Course: Simulation of Physical and Weapon Systems, Naval Postgraduate School, Monterey, CA, 2010.

[4] "Free Electron Laser," n.d., Wikipedia, the free encyclopedia, http://en.wikipedia.org/wiki/Free_electron_laser (accessed October 7, 2009).

[5] "Gaussian Beam," n.d., Wikipedia, the free encyclopedia, http://en.wikipedia.org/wiki/Gaussian_beam (accessed March 19, 2010).

[6] "Attenuation," n.d., Wikipedia, the free encyclopedia, Available: http://en.wikipedia.org/wiki/Attenuation (accessed February 9, 2010).

[7] C. McGee et al., "Transparency of atmosphere at sea level." *IEEE Trans. Antennas Propag.,* vol. 49, p. 1683, 2001.

[8] F. G. Gebhart, "Nonlinear propagation: Thermal blooming," *IR/EO Systems Handbook, Atmospheric Propagation of Radiation, Vol. 2,* Bellingham, WA: SPIE Optical Engineering Press, 1993.

[9] C. Freudenrich, March 31, 2008. "How Laser Weapons Work." HowStuffWorks.com. Available: http://science.howstuffworks.com/laser-weapon.htm (accessed May 3, 2010).

[10] ESCO products, n.d., *Sapphire Material Data*. Available: http://www.escoproducts.com/html/sapphire.html (accessed January 19, 2010).

[11] Kyocera, n.d., "Single crystal sapphire." Available: http://global.kyocera.com/prdct/fc/product/pdf/s_c_sapphire.pdf (accessed November 18, 2009).

[12] Rocky Mountain Instrument Co., n.d., *Optical Materials Selection Guide*. Available: http://rmico.com/technical-notes/transmission-curves (accessed March 21, 2010).

[13] TYDEX J.S.Co., n.d., "HRFZ silicon material data." Available: http://www.tydexoptics.com/en/materials/for_transmission_optics/silicon/ (accessed March 9, 2010).

[14] Korth Kristalle GMBH, n.d., "Zinc selenide." Available: http://www.korth.de/eng/503728952d091450d/503728952d0c26651.htm (accessed March 17, 2010).

[15] Janos Technology., n.d., *ZnSe Optical Material Guide.* Available: http://www.janostech.com/knowledge_center/znse_material.html (accessed January 6, 2010).

[16] Diamond Materials., n.d., *The CVD Diamond Booklet.* Available: http://diamond-materials.com/properties_en.htm (accessed January 6, 2010).

[17] V. V. Kubarev, "Optical properties of CVD-diamond in terahertz and infrared ranges." *Nuclear Inst. and Methods in Phys. Research*, vol. A 603, pp. 22-24, 2009.

[18] M. W. Zemansky, *Heat and Thermodynamics (5th Edition)*. New York: McGraw Hill, 1968.

[19] W. B. Colson et al., *Free Electron Laser Handbook*. Amsterdam, The Netherlands: Elsevier Science Publishing Company, Inc., 1990.

[20] P. Crooker et al., "Short rayleigh length free electron laser: Experiments and simulations," *Phys. Rev. Special Topics–Accelerators and Beams* vol. 11, no. 090701, 2008.

[21] S. P. Niles, Lieutenant Commander, United States Navy,
     (private communication), May 18, 2010.

THIS PAGE INTENTIONALLY LEFT BLANK

INITIAL DISTRIBUTION LIST

1. Defense Technical Information Center
   Ft. Belvoir, Virginia

2. Dudley Knox Library
   Naval Postgraduate School
   Monterey, California

3. Chairman, Department of Physics
   Naval Postgraduate School
   Monterey, California

4. Prof. William B. Colson
   Naval Postgraduate School
   Monterey, California